CrossMark

REGULAR PAPER

Athanasia Kalpakli Vester · Sohrab S. Sattarzadeh ·
Ramis Örlü

Combined hot-wire and PIV measurements of a swirling turbulent flow at the exit of a 90° pipe bend

Abstract Measurements of turbulent swirling flow by means of hot-wire anemometry and stereoscopic particle image velocimetry were performed, 0.67 pipe diameters downstream a 90° pipe bend. The flow for a wide range of swirl numbers up to $S = 1.2$, based on the angular velocity of the pipe wall and bulk velocity, was investigated and compared to the non-swirling case. The limitations and advantages of using a single hot-wire probe in a highly complex flow field are investigated and discussed. The present paper makes available a unique database for a kind of flow that has been neglected in literature and which is believed to be useful for validation purposes for the computational fluid dynamics community.

Keywords Turbulent pipe flow · Swirling flow · Hot-wire anemometry · Particle image velocimetry

1 Introduction

Turbulent flow in curved pipes has for long captured the interest of the fluid physics community both from an applied (Ono et al. 2010) and fundamental point of view (Hüttl and Friedrich 2001). Curved pipes can be found as part of almost any mechanical system, e.g., nuclear reactors (Yamano et al. 2011; Yuki et al. 2011), heat exchangers (Chang 2003) and reciprocating engines (Hellström 2010; Kalpakli et al. 2012, 2013). Pipe bends are hence widely used due to space limitations (a compact packaging and reducing engine capacity is of great importance, for example, in vehicle design) but also due to the need for altering the direction of the fluid motion. Laminar flow through curved pipes has been studied in detail throughout the years and it is mostly associated to physiological or biological systems (Helps and McDonald 1954; Chandran and Yearwood 1981; Glenn et al. 2012) and it is not the scope of the present paper. From a technical or applied point of view, the focus lies on turbulent flows in bent pipes (Vashisth et al. 2008) and so far a number of techniques (both computational and experimental) have been utilised to be able to understand some of its characteristics. The flow through curved pipes is three dimensional and exhibits a strong secondary motion in the form of two counter-rotating vortices, so-called Dean cells/vortices (Dean 1927). Under turbulent flow conditions these vortices have been found to exhibit a low-frequency oscillation causing fatigue in piping systems (Tunstall and Harvey 1968; Rütten et al. 2005). Moreover, the strength of the secondary flow is known to depend on

A. Kalpakli Vester (✉) · R. Örlü
KTH CCGEx - Competence Centre for Gas Exchange, SE-100 44 Stockholm, Sweden
E-mail: sissy@mech.kth.se
Tel.: +46-8-7906192

A. Kalpakli Vester · S. S. Sattarzadeh · R. Örlü
Linné FLOW Centre, KTH Mechanics, Royal Institute of Technology, SE-100 44 Stockholm, Sweden

the inlet boundary layer (Enayet et al. 1982) and measurements upstream and across 180° bends have shown an increase in energy production due to extra strain rates induced by curvature. The effects of curvature have been found to persist more than 18 diameters downstream the bend exit (Anwer et al. 1989).

The turbulent flow in a curved pipe is complex and to understand its dynamics experimental methods need to be combined, so that information is obtained both on the large-scale structures but also statistics of the flow. To date, there is no experimental study—to the authors' knowledge—which provides information from both sides of the spectrum and could also serve as a test case for validation of turbulence models, i.e., so far either the unsteady behavior of the Dean vortices is investigated by means of whole-field techniques which cannot fully resolve the smaller scales of turbulence (Brücker 1998; Sakakibara and Machida 2012; Kalpakli and Örlü 2013; Hellström et al. 2013) or single-point measurements are performed in order to provide converged statistics (Enayet et al. 1982; Azzola et al. 1986; Sudo et al. 1998). Simulations of such flows are favored, but on the other hand those highly depend on the grid resolution and do not always model the flow correctly (Al-Rafai et al. 1990; Hellström 2010). In particular, the flow case of turbulent flow through a 90° bend is often employed as a test case for turbulence models (Kadyirov 2013) and large-eddy simulations (LES) (Fjällman et al. 2013; Carlsson 2014; Röhrig et al. 2015). Hence, there has been a great demand, both in the past and at present, for validation of turbulence models through comparisons with experimental data of such flows (Boersma and Nieuwstadt 1996; Rütten et al. 2005; Pruvost et al. 2004). An exception is the direct numerical simulations (DNS) which on the other hand demand a high computational cost and so far have only been performed for flows in a torus (Hüttl and Friedrich 2001; Noorani et al. 2013; Noorani and Schlatter 2015).

In addition to the above, a field which has been neglected in the literature is the effects of a swirling flow superimposed on the turbulence in a curved pipe. In such a case a Coriolis force acts on the fluid and the balance between centrifugal, inertial and viscous forces in the curved pipe changes. Swirling flow is met in a variety of industrial processes wherever a fan or rotating element or multiple of bent pipe sections (Yuki et al. 2011) is present. Furthermore, turbulent swirling flow is encountered in many engineering applications such as cyclone separators, gas combustors and pipeline complexes (for examples see Jakirlić et al. 2002). Note that a number of different methods (rotation, tangential injection and vanes) exist for the generation of swirl which have a different effect on the base flow. For details the reader is referred to Örlü (2009). Here we focus on the rotation method, which was employed in the present study, i.e., through axially rotating the straight pipe section, since it provides a well-defined velocity profile and does not leave traces of the swirl generating mechanism (such as other means to introduce swirl on the flow).

Swirling flow imposed on turbulent pipe flow is known to decrease the pressure drop (White 1964)—and consequently the friction factor—and create less full shaped mean streamwise velocity profiles, i.e., the centreline velocity increases and the velocity gradient at the wall decreases, thereby approaching the one of a laminar flow (Murakami and Kikuyama 1980; Reich and Beer 1989). In such a case, the fluid is not in solid body rotation due to the influence of the cross-stream Reynolds stress and the azimuthal velocity profile is nearly parabolic (Kikuyama et al. 1983b; Imao et al. 1996; Facciolo et al. 2007). Coupled to this, increase in the swirl intensity has been shown to decrease the turbulence intensity (Kikuyama et al. 1983a; Imao et al. 1996). Some empirical relations for friction factors in swirling turbulent and laminar flow can be found in Ito and Nanbu (1971). More recent three-dimensional laser Doppler velocimetry measurements of turbulent swirling straight pipe flow (Rocklage-Marliani et al. 2003), showed an annihilating effect of the swirl on the Reynolds shear stresses, i.e., the Reynolds stresses were found to be low in the pipe core region, therefore suggesting that the swirl tends to laminarise the flow, however, only regarding the mean azimuthal velocity. One of the first LES performed on turbulent swirling flow (Eggels 1994) confirmed the above and showed that the largest increase in the turbulence intensity is observed for the streamwise velocity component. Early DNS (Orlandi and Fatica 1997) showed that the reduction in drag is responsible for a widening of the near wall structures in a turbulent swirling straight pipe flow. Those data were used later by Feiz et al. (2003) in order to show that LES can reasonably well predict phenomena in rotating turbulent pipe flow. Reynolds stress models were developed by Speziale et al. (2000) and were successful in capturing the main features of turbulent swirling flow as described above. More recent DNS on turbulent swirling flow in a straight pipe (Nygård and Andersson 2009) have shown the effect of swirl on near wall structures which appear as elongated streaks being tilted and shortened as the swirl intensity increases.

When it comes to turbulent swirling flow in a curved pipe, and more specifically to pipes which are 90° bend, the information available is limited. One of the few studies conducted in swirling turbulent flow in a 180° bend is the one by Anwer and So (1993). Mean streamwise velocity distributions downstream the bend showed that for the swirling flow case, the profiles were more uniform and symmetric. This suggested that a single dominating cell exists for a sufficiently high swirl intensity and that the curved pipe flow becomes

fully dominated by the imposed swirl. The follow-up work by So and Anwer (1993b) showed that in swirling flow, the distance needed for the flow to become fully developed is shorter in a curved pipe compared to a straight pipe. Furthermore, it was found that the bend accelerates the decay of the swirl. Some of those findings were later confirmed numerically by Pruvost et al. (2004) and it was shown that one of the Dean vortices which has the same direction of rotation as the imposed swirling motion gets strengthened. As the swirl intensifies, the Dean cells tend to merge in a single cell until the flow field becomes completely swirl dominated and the mean axial velocity profile is symmetric. Similar observations were made by Kalpakli et al. (2012), Kalpakli and Örlü (2013) and Kalpakli Vester et al. (2015) by means of particle image velocimetry (PIV), where a modal analysis additionally revealed that there might be structures, similar to the Dean cells, underlying the swirl dominated flow field. In the same study a similar behavior of the large-scale structures as in the DNS by Nygård and Andersson (2009) for a straight pipe, was also observed. At this point, we should also mention studies conducted in turbulent curved pipe flow that generated the swirling motion using guided vanes or tangential inlet, even though the effects of the swirl on turbulence in such case might differ from the present study. One of the earlier studies on swirling flow is the one by Binnie (1962) who experimentally observed the motion of a fluid particle which is in contact with the pipe wall, in a turbulent swirling flow through a bend. Using a pitot tube, Shimizu and Sugino (1980) investigated hydraulic power losses in a 180° bend. The difference in the formed flow patterns in the case when the imposed swirling motion is a free- or forced-type vortex was also investigated. Those data were later used to validate a theoretical study in swirling curved pipe flow (Kitoh 1987). Last, a noticeable study is the one by Chang and Lee (2003) where the swirling turbulent flow through a 90° bend was investigated using two-dimensional PIV. The main results consisted of mean axial velocity profiles and axial root mean square (r.m.s.) distributions. Due to the swirl generating method (tangential inlet), and high swirl intensity, high axial velocity near the pipe wall and negative velocity at the pipe core was reported at the pipe inlet. As the swirl decayed along the bend, the maxima of the mean axial velocity shifted to the convex pipe wall until a bend angle of 45 degrees and thereafter shifted again towards the concave pipe wall.

Table 1 shows few of the works which have been conducted in turbulent swirling flows in straight pipes as well as non swirling turbulent flows in pipe bends while—to the authors' knowledge—*all* of the studies done on turbulent swirling flows in bends are listed. The latter highlights the lack of studies in turbulent swirling flows in curved pipes. Hot-wire data in swirling turbulent curved pipe flow became available for validation of Computational Fluid Dynamics (CFD) codes by So and Anwer (1993a), however only for one swirl intensity, which does not cover the swirl-dominated case as stated in Pruvost et al. (2004): "Lack of experimental data does not allow the validation of the predictions for so high values of the swirl intensity, but results are of qualitative interest to illustrate the flow behavior in the bend when motion is swirl-dominated." Furthermore, it should be highlighted that, the data provided by So and Anwer (1993a), Anwer and So (1993) and So and Anwer (1993b) regard a case where the swirl is decaying along the pipe, therefore those are not the most suitable databases for validation of CFD codes, where a well-defined inflow condition

Table 1 Studies of turbulent flows in straight and curved pipes with and w/o swirl

Flow in bends	Swirling flow in straight pipes	Swirling flow in bends
Tunstall and Harvey (1968)	White (1964)	Binnie (1962)
Enayet et al. (1982)	Murakami and Kikuyama (1980)	Shimizu and Sugino (1980)
Azzola et al. (1986)	Kikuyama et al. (1983a)	Anwer and So (1993)
Anwer et al. (1989)	Kikuyama et al. (1983b)	So and Anwer (1993a)
So and Anwer (1993b)	Reich and Beer (1989)	So and Anwer (1993b)
Boersma and Nieuwstadt (1996)	Eggels (1994)	Chang and Lee (2003)
Brücker (1998)	Imao et al. (1996)	Pruvost et al. (2004)
Sudo et al. (1998)	Orlandi and Fatica (1997)	Kalpakli and Örlü (2013)
Hüttl and Friedrich (2001)	Speziale et al. (2000)	
Pruvost et al. (2004)	Rocklage-Marliani et al. (2003)	
Rütten et al. (2005)	Feiz et al. (2003)	
Hellström (2010)	Facciolo et al. (2007)	
Sakakibara and Machida (2012)	Nygård and Andersson (2009)	
Fjällman et al. (2013)	–	
Noorani et al. (2013)		
Kalpakli and Örlü (2013)		
Hellström et al. (2013)		
Carlsson (2014)		
Röhrig et al. (2015)		
–		

is needed. Therefore, the aim of the present work is to provide experimental data of turbulent swirling flow downstream a 90° bend, for a wide range of swirl intensities and from a setup which allows well-defined inflow conditions, i.e., as it will be explained later on, here the swirl is generated by axially rotating the *whole* pipe. Time-resolved stereoscopic particle image velocimetry (TS-PIV) as well as hot-wire anemometry (HWA) measurements were performed at the exit of a 90° pipe bend for a wide range of swirl intensities, providing information on the large-scale structures and turbulence statistics, respectively. Such a data base is—to the author's knowledge—not available in the literature, and will be of use for validation purposes for the CFD community, as can be appreciated from the studies by Fjällman et al. (2013), Carlsson (2014), Röhrig et al. (2015) and Pruvost et al. (2004).

2 Experimental facility and measurement techniques

In the following section the experimental facility and measurement techniques will be presented.

2.1 Rotating pipe facility

The measurements (both PIV and HWA) were performed in the rotating pipe facility located at the Fluid Physics Laboratory at KTH Mechanics. The facility mainly consists of a 100 pipe diameter (D) long axially rotating pipe. Figure 1a shows a schematic of the rotating pipe facility. Air at ambient temperature is provided by a centrifugal fan (A) with a butterfly valve for flow rate adjustment, which is monitored through the pressure drop across an orifice plate (B) inserted in the air supply pipe. A distribution chamber (D) to reduce the transmission of vibrations generated by the fan is mounted on the way. From there the air stream is distributed into three different spiral pipes, which are symmetrically fed into the stagnation chamber (E), consisting of a honeycomb, in order to distribute the air evenly. One end of the cylindrical stagnation chamber is covered with an elastic membrane in order to further reduce the pressure fluctuations. A bell mouth shaped entrance first leads the air into a one meter long stationary section, which is connected to the rotating pipe (K) through a rotating coupling (F). In the first section of the rotating part of the pipe a 12 cm long honeycomb (G), consisting of drinking straws of a diameter of 5 mm, is mounted which brings the flow into more or less solid body rotation. The inner diameter of the pipe (D) amounts 60 mm whereas the wall thickness is 5 mm. The 6 m long pipe is made of seamless steel and has a honed inner surface with a roughness of less than 5 micron, according to manufacturer specifications. It is supported along its full length by five ball bearings (J), which are mounted within a rigid triangular shaped framework. The pipe is belt driven via a feedback controlled DC motor (H), which is capable to run the pipe up to rotational speeds of 2000 rpm. For more information on the facility the reader is referred to Facciolo (2006). At the exit (M) of the long steel pipe a 90° bent pipe is connected (Fig. 1b). Note that in case of rotation, the entire 6 m long straight pipe rotates along its axial direction, while the bend remains fixed. The bend has a centreline radius, R_c equal to 1.5D yielding a curvature ratio R/R_c of 0.31, where R the pipe radius. The length of the straight section after the 90° curvature
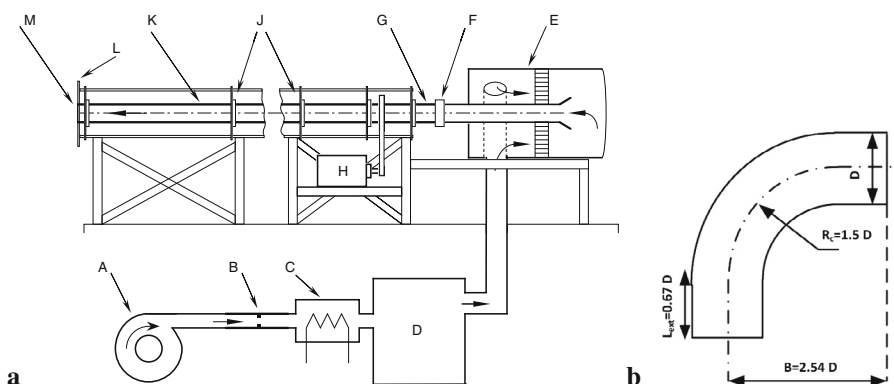

Fig. 1 a Schematic of the rotating pipe facility at KTH Mechanics. *A* Centrifugal fan, *B* flow meter, *C* electrical heater, *D* distribution chamber, *E* stagnation chamber, *F* coupling between stationary and rotating pipe, *G* honeycomb, *H* DC motor, *J* ball bearings, *K* rotating pipe, *L* circular endplate, *M* pipe outlet to which the pipe bend (**b**) has been mounted. **b** Pipe bend with inner diameter $D = 60$ mm

is 0.67 D and all measurements were done exactly at this station. As apparent from Fig. 1 the pipe flow (both for the straight and pipe bend) emanates into the still ambient air. It should be noted that parts of the presented data here, have been utilised in previous work by the authors (Kalpakli and Örlü 2013), however, the data has not been described and discussed with respect to turbulence statistics before.

2.2 Hot-wire anemometry

The hot-wire measurements were done using a Platinum wire with nominal diameter of 5 micron and length of 1 mm, respectively, which was soldered on straight prongs. The single wire hot-wire was fixed in a 300 mm long probe holder that was mounted on an airfoil shaped arm in order to minimize the upstream effects of the probe and the probe holder on the flow. The hot-wire was calibrated *ex-situ* in a calibration nozzle against a FCO12 (Furness Controls, used in 10 % FS, i.e. 200 Pa with ± 0.5 % accuracy of reading) micro manometer. The hot-wire anemometer system used is a Dantec StreamLine 90N10 frame in conjunction with a 90C10 constant temperature anemometer module. The hot-wires were operated in constant temperature anemometry mode at an overheat resistance ratio of 80 %. Mass flow rate and temperature of the flow were monitored and the instantaneous velocity was compensated for possible temperature variations as described in Örlü and Alfredsson (2007). The sampling frequency was set to 20 kHz in order to obtain converged statistics.

2.3 Time-resolved Stereoscopic Particle Image Velocimetry (TS-PIV)

For the TS-PIV measurements, a high-speed PIV system consisting of a Nd:YLF laser (Pegasus, 10 kHz maximum repetition rate, New Wave Research) and two C-MOS cameras (Fastcam APX RS, Photron, 3000 fps at 1024×1024 px^2) was used. The laser light sheet was aligned exactly at the pipe outlet (approximately 0.5 mm from the exit) as shown in Fig. 2. It should be noted here that the chosen experimental tactic, i.e., perform measurements at the pipe outlet and not inside the pipe, was chosen due to the challenges imposed by the necessity for correction for aberrations due to the circular shape of the pipe and the viewing angle of the two cameras and obtaining a good resolution with air as a fluid medium when performing PIV measurements. This, however, does not oppose restrictions of using the present data for CFD validation purposes, as apparent from the LES studies by Fjällman et al. (2013) and Röhrig et al. (2015). For the seeding of the flow, a water-based solution (Jem Pro Smoke Super ZR-Mix) was atomised using a high volume liquid seeding generator (10F03 Seeding Generator, DANTEC), placed at the inlet of the centrifugal fan (A in Fig. 1). For the *in-situ* calibration of the cameras, images were taken of a two-level calibration plate positioned at the measurement plane. A self-calibration procedure has been applied to eliminate errors from misalignment of the laser light sheet with the calibration target (Wieneke 2005).

The raw images from the measurements had a resolution of 1024×1024 px^2 at 10-bit while the field of view was equal to 80×80 mm^2 in physical space. For the non-swirling cases, $N_s = 3000$ images were acquired whereas 1000 images were acquired for the rest of the cases at a sampling frequency, f_s, of 1 kHz.

The post-processing of the PIV data was performed using DaVis 7.2 (LaVision GmbH). The vector fields were calculated through a multi-pass correlation iteration procedure in order to increase resolution, starting
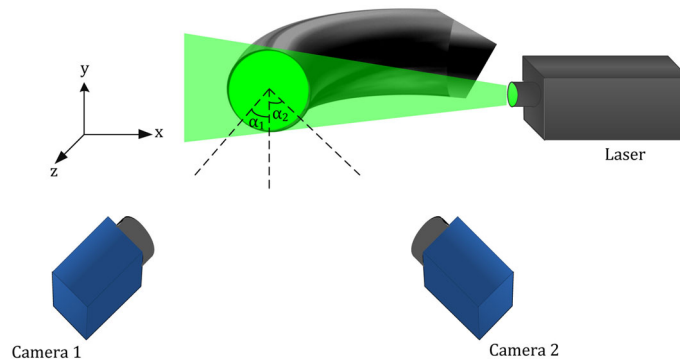

Fig. 2 TS-PIV setup with the laser light sheet aligned exactly at the pipe outlet due to limited optical access. The angles in-between the cameras, denoted as α_1 and α_2 were approximately 45° each

Table 2 Parameter range for the experiments

Pipe	$Re_D \times 10^{-3}$	S	HWA	SPIV
Straight	24	0, 0.1, 0.3, 0.5	✔	
Bend	14	0	✔	
Bend	24	0, 0.1, 0.3, 0.5	✔	✔
Bend	34	0	✔	✔
Bend	14	0, 0.85, 1.2		✔

with a $64 \times 64 \, \text{px}^2$ interrogation window and decreasing to $16 \times 16 \, \text{px}^2$ interrogation (which sets also the lower limit for the spatial resolution) window with $50\,\%$ area overlapping. The percentage of accepted vectors was more than $95\,\%$. In all the cases a median test (Westerweel 1994) has been used to detect outliers and replaced by a linear interpolation of the neighboring vectors.

3 Flow parameters

Two non-dimensional parameters will be used throughout this paper and their definitions are given in the following.

The *Reynolds number* is given based on the bulk velocity (W_b) and pipe diameter:

$$Re_D = \frac{\rho W_b D}{\mu}, \tag{1}$$

where ρ denotes density and μ the dynamic viscosity of the fluid medium (air).

With the present experimental setup, the mean velocity both in axial and tangential direction is well defined by rotating the entire straight pipe section, in which case the integral swirl number (see Gupta et al. (1985) for definition) can be interchanged with the *swirl number* defined as:

$$S = \frac{U_w}{W_b}, \tag{2}$$

with U_w being the angular velocity of the pipe wall. This is a convenient way to define the swirl number since the wall velocity can be directly obtained by the rotational speed of the pipe which is monitored in the present experimental apparatus. The pairs of swirl and Reynolds numbers shown in the present study with the HW and TS-PIV measurements are listed in Table 2.

4 Results

In the following sections, results from turbulent flow $0.67D$ downstream a curved pipe, with and without swirl, will be presented. Some results from turbulent straight pipe flow will also be shown for the description of the inflow conditions. Note that for all results presented, the coordinate system shown in Fig. 2 is used, with z being the streamwise, x the horizontal and y the vertical directions corresponding to W, U and V velocity components, respectively. Capital letters denote time-averaged quantities, whereas primed small letters denote rms quantities.

4.1 Data quality

The flow at the the exit of the long pipe (see M in Fig. 1) is a fully developed turbulent pipe flow. Figure 3a shows the mean velocity profiles for different swirl intensities, whereas Fig. 3b shows the corresponding r.m.s., at $Re_D = 24,000$ at the exit of the straight long pipe. The profile for the non-swirling case, compared to DNS data by Wu and Moin (2008), depicts a fully developed turbulent pipe flow, while as the swirl number increases the profile approaches that of laminar flow (Facciolo 2006; Shirvan 2011); for inner-scaled quantities from the same experimental facility, the reader is referred to Örlü and Alfredsson (2012). It is also observed that with increasing swirl number the imposed motion is dominating the turbulent flow which can be seen in Fig. 4, where the effect of swirl on the ratio between centreline and bulk velocity is shown. Data
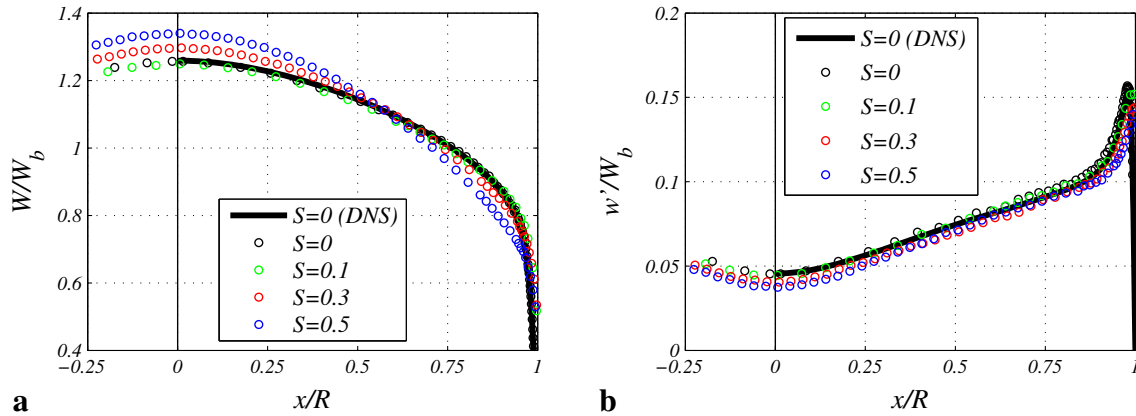
Fig. 3 Swirl number effect on the **a** mean streamwise velocity and **b** r.m.s. profiles normalized by the bulk velocity, in the straight pipe flow at $Re_D = 24,000$. *Black thick line* is DNS data at the same Reynolds number (Wu and Moin 2008)
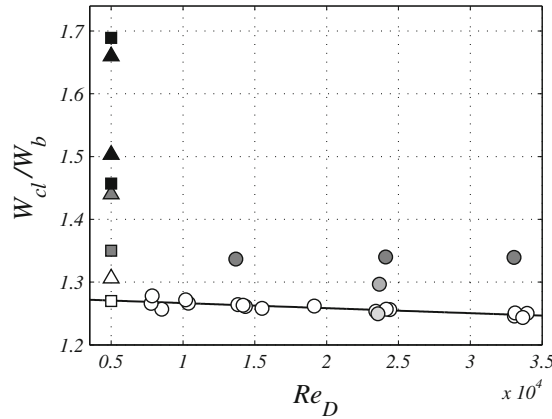

Fig. 4 Effect of the Reynolds number and swirl number on the ratio between the centerline velocity and the bulk velocity, for the straight pipe flow. The *square* symbols are the experimental results from Reich and Beer (1989), the *triangular symbols* are DNS by Orlandi and Fatica (1997), and the *circular symbols* are the data from the present study. *Darker symbols* are representing higher swirl numbers and *open symbols* denote different flow cases (Reynolds numbers)

from DNS is also included to expand the swirl number range. This ratio is increasing with swirl number, whereas it displays a very weak dependence on the Reynolds number.

In order to assess how well the single hot-wire measures downstream the bend, i.e., in a three-dimensional flow field, the streamwise velocity profiles in the horizontal plane taken with the hot-wire for three swirl numbers were compared to the corresponding TS-PIV data. When no swirl is imposed on the flow, a difference between the data obtained from the two experimental techniques is observed at the inner bend wall, see Fig. 5a. The single hot-wire senses the so-called effective cooling velocity ($W_{\text{eff}} = \langle \sqrt{w^2 + h^2 u^2 + k^2 v^2} \rangle$, where h and k denote the pitch and yaw factor, $\langle \cdot \rangle$ is the time-average operator and small letters denote instantaneous absolute quantities) (Bruun 1995) and therefore the error introduced by the in-plane motion is higher closer to the inner wall where the in-plane components are comparably large with respect to the streamwise component. If, instead, the effective cooling velocity is computed from the PIV data and plotted against the HW data, then the agreement is improved as is clearly depicted in Fig. 5b. Note that the single hot-wire here is aligned vertically to the flow direction, therefore the largest error is introduced by the u-velocity component (which acts as the bi-normal cooling velocity). It is noticeable also that as the swirl number increases, the agreement between the "actual" PIV data (i.e., not the effective cooling velocity) and HW data becomes better. That is explained by the fact that by increasing the swirl intensity the effects from the bend become weaker (Pruvost et al. 2004; Kalpakli and Örlü 2013) and the streamwise velocity increases compared to the in-plane velocities. This can clearly be seen also in Fig. 6a, where the angle defined as $\theta = \arctan\langle u/w \rangle$ is plotted from the TS-PIV data for increasing swirl
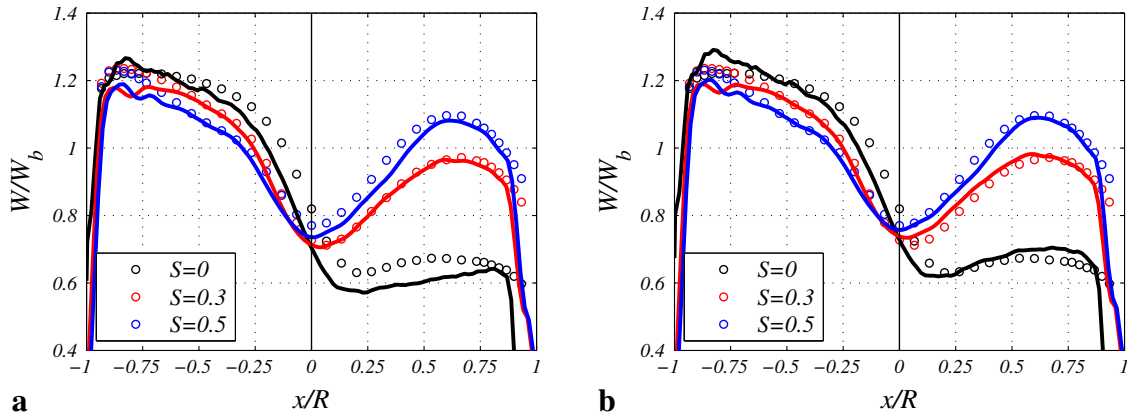
Fig. 5 a Comparison of mean streamwise velocity component along the horizontal plane from the TS-PIV (*lines*) and HW (*circles*) data at $Re_D = 24,000$ and $S = 0, 0.3, 0.5$. **b** Same as **a**, but here the effective cooling velocity ($W_{eff} = \langle \sqrt{w^2 + h^2 u^2 + k^2 v^2} \rangle$) calculated from the TS-PIV data is plotted against the HW data. Note that the effective cooling velocity is the one sensed by the single HW (therefore it is used for comparisons here) but it is calculated from PIV data
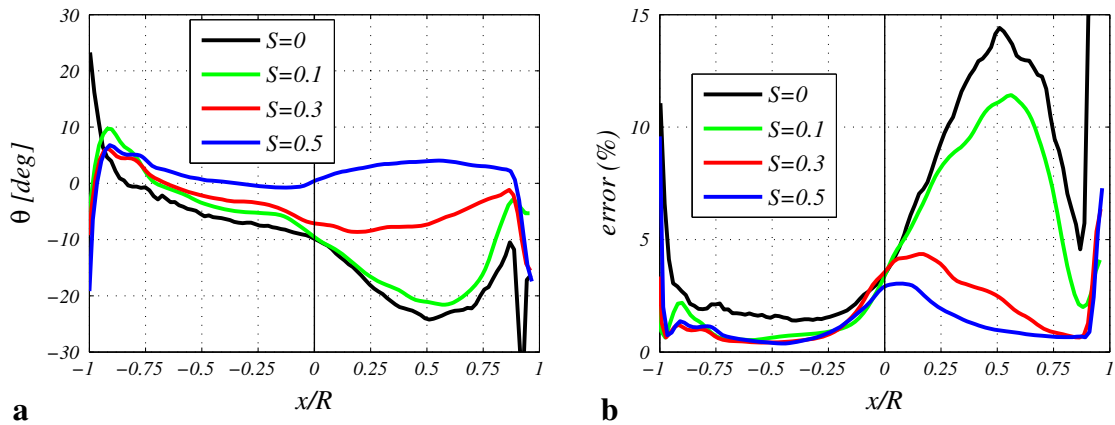
Fig. 6 a The angle $\theta = \arctan\langle u/w \rangle$ for $S = 0, 0.1, 0.3$ and 0.5 from the TS-PIV data at $Re_D = 24,000$. Increased colour intensity indicates increased swirl number. **b** Percentage error of the hot-wire readings defined as $(W_{eff} - W)/W$ for $S = 0, 0.1, 0.3$ and 0.5 from the TS-PIV data at $Re_D = 24,000$

numbers. It is observed that the angle across the horizontal pipe axis approaches zero at the centreline and the whole profile becomes more symmetric, as the swirl number increases. Additionally, the percentage error of the hot-wire readings is plotted for each swirl number and position along the horizontal pipe axis in Fig. 6b. It can clearly be seen that this error is larger close to the inner wall for the non-swirling flow case (at highest approximately 15 %), whereas it drops significantly with increase in swirl number. This provides the confidence that the data obtained with the single hot-wire can be used for an accurate statistical analysis of the turbulent swirling pipe flow studied here.

Furthermore, in order to assure that taking the PIV data at the pipe outlet would provide representative data compared to those taken inside the pipe, the same PIV data for $S = 0$ showed in the previous figure, were plotted against hot-wire data which were taken inside the pipe with a $1D$ pipe extension mounted downstream the measurement plane. The results in Fig. 7 shows that, for at least a statistical description of the flow field for the measurement points provided here, this measurement tactic provides representative data for data taken within the pipe.
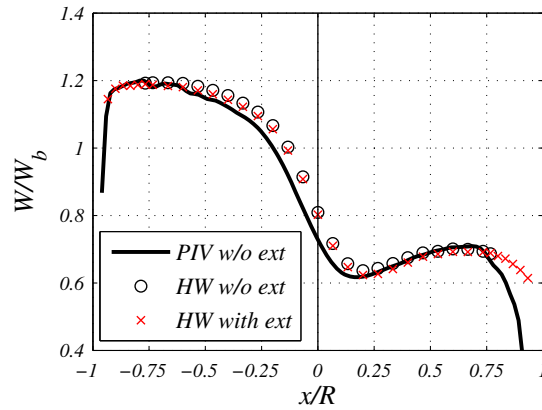
Fig. 7 Mean streamwise velocity component along the horizontal plane. Line indicates the effective cooling velocity from the TS-PIV data, circles the HW data and red crosses are HW data taken with a $1D$ extension mounted downstream the measurement plane
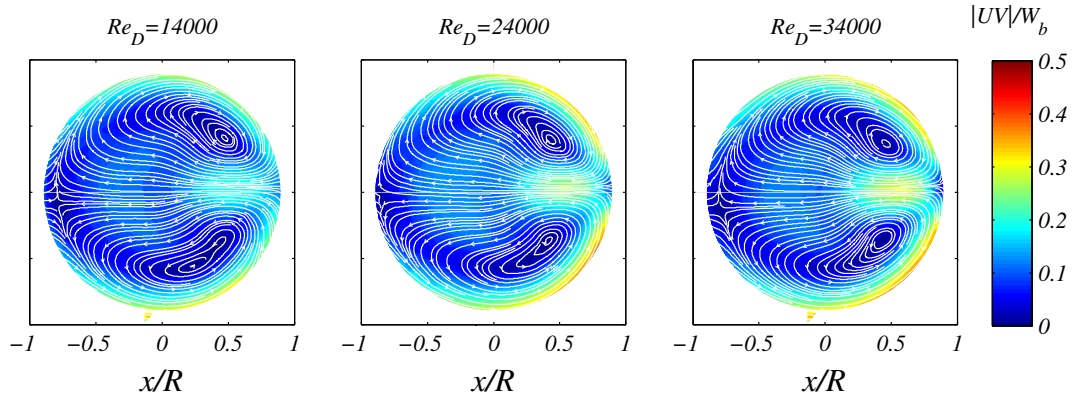

Fig. 8 Magnitude of in-plane components ($|UV| = \sqrt{(U^2 + V^2)}$) scaled by the bulk velocity shown as the contour map and in-plane components shown as sectional streamlines for three Reynolds numbers ($Re_D = 14,000, 24,000, 34,000$)

4.2 Reynolds number effect on the time-averaged flow field

The magnitude of the in-plane components for three Reynolds numbers ($Re_D = 14,000, 24,000, 34,000$) from the TS-PIV data, is shown in Fig. 8 as contour map together with the in-plane velocities as the imposed sectional streamlines. In all three cases the Dean vortices are clearly depicted forming two bean-like shaped symmetrical cells around the pipe horizontal axis. It can be clearly seen that with increase in Reynolds number, the in-plane velocities increase in strength and especially at the inner pipe wall. The mean streamwise velocity profiles of the above cases acquired with the single HW are shown in Fig. 9a, whereas the r.m.s. is shown in Fig. 9b. Here, it is again clear that there is an effect of Reynolds number at the inner wall of the curved pipe. In particular the velocity increases at the inner bend with increasing Reynolds number indicating that the bend effects are more profound with increasing Re_D since it leads to a more skewed velocity profile. The r.m.s. however does no depict significant differences between the three Reynolds numbers. This indicates also that the error of the single hot-wire readings will increase with increase in Re_D due to the higher values of the u-velocity component (see previous section).

4.3 Swirl number effect

The magnitude of the in-plane components, similarly to Fig. 8 is shown in Fig. 10 this time for different swirl numbers from $S = 0$ to $S = 1.2$ (the corresponding Reynolds numbers can be found in Table 2). The behavior of the Dean vortices which is illustrated has been described in Kalpakli and Örlü (2013) and it is as follows: with a slight increase in swirl intensity ($S = 0.1$) a perturbation of the flow symmetry is observed.
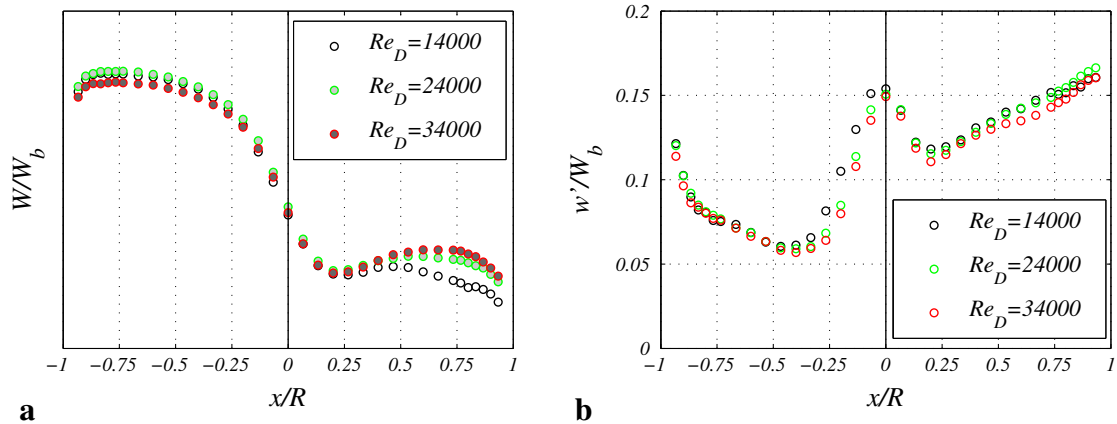
Fig. 9 The Reynolds number effect on the **a** mean streamwise velocity and **b** r.m.s. profile normalized by the bulk velocity
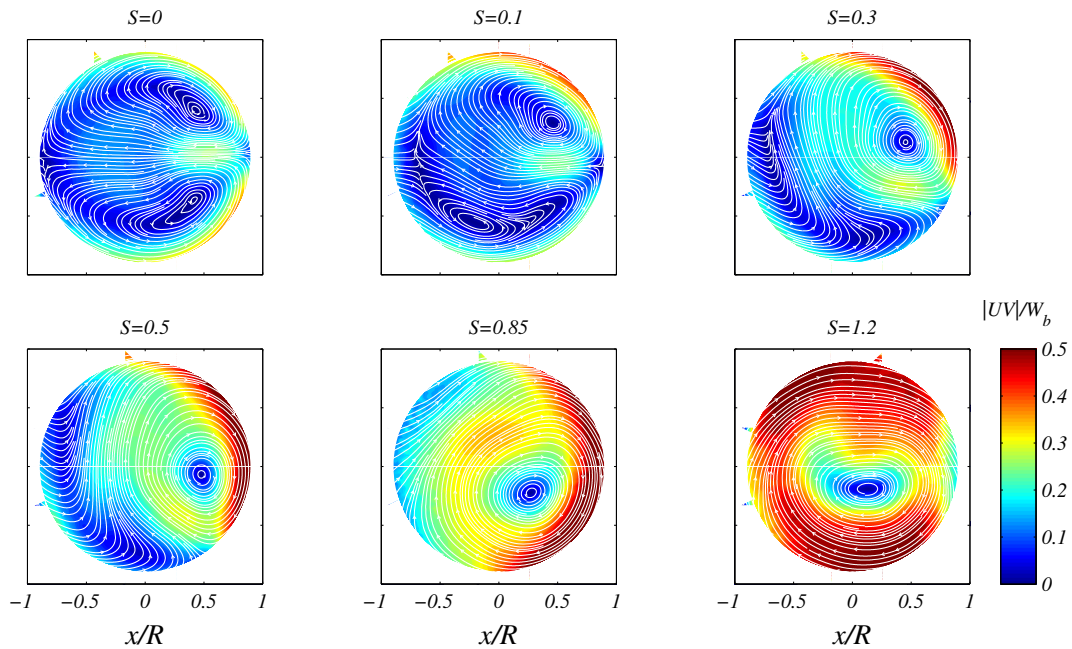

Fig. 10 Same quantities and color coding as in Fig. 8 for different swirl numbers: $S = 0, 0.1, 0.3, 0.5, 0.85$ and 1.2. A movie of the present figure with an interval of 1 ms and real-time length of 50 ms is supplemented as an Online Resource

The upper vortex which rotates at the same direction as the imposed swirling motion (clockwise), gets strengthened and gradually dominates the flow field as the swirl number increases, whereas the lower vortex has already been dispersed at $S = 0.3$. At the highest swirl number shown here, the flow field is dominated by a single vortex which spans the whole cross-section and is located slightly off-centre towards the lower pipe wall. It is interesting to note that the centre of the single vortex at $S = 1.2$ is found to be located slightly off-centre and towards the lower side of the pipe. From theory, since this vortex is a result of the upper Dean vortex merging with the applied solid-body rotation it would be expected that the centre of it at the highest swirl number is located towards the upper side of the pipe instead. This can probably be explained by the curvature effects on the upstream of the bend flow field, which create a non-symmetrical azimuthal velocity profile fed into the bend.

Figure 11 illustrates mean streamwise velocity profiles along the horizontal pipe axis for different swirl numbers and $Re_D = 24,000$, from the HW data. It is shown that by increasing the swirl number, as the flow is becoming swirl dominated, the effect of pipe curvature is decreasing in the mean velocity profiles. The
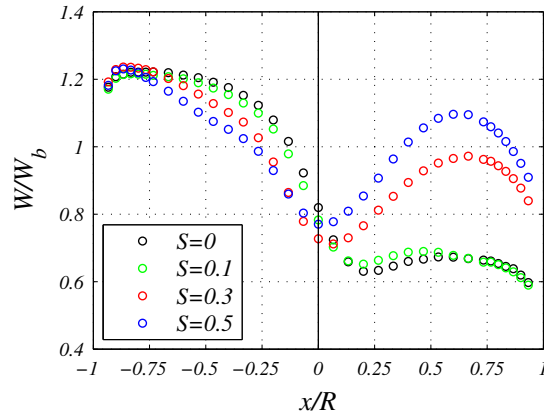
Fig. 11 The swirl number effect on the mean streamwise velocity profiles normalized by the bulk velocity at $Re_D = 24,000$
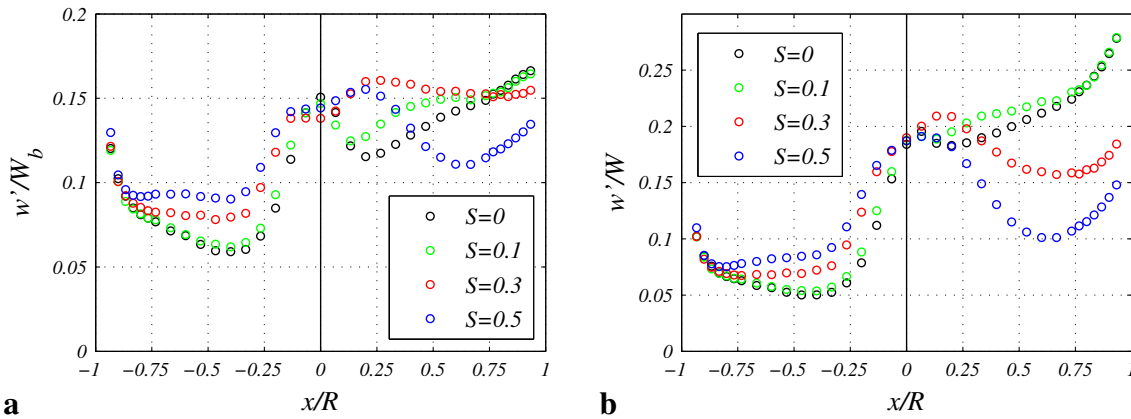

Fig. 12 The swirl number effect on the **a** outer-scaled streamwise r.m.s. and **b** turbulence intensity at $Re_D = 24,000$

pipe curvature effects downstream the bend exit is smoothened both in outer and inner parts of the bend exit considerably for $S = 0.3$ and 0.5. The r.m.s. and turbulence intensity for the same cases are shown in Fig. 12a and b, respectively. It is clear that as the swirl number increases, the turbulence intensity decreases at the inner wall of the curved pipe, whereas for the outer wall the opposite occurs.

5 Summary and conclusions

This paper provides for the first time—to the authors' knowledge—an extensive database for swirling turbulent curved pipe flow which has been missing from the literature. Turbulent swirling flow at the exit of a pipe bend was studied both by means of stereoscopic PIV and hot-wire anemometry. A wide range of swirl numbers was employed by axially rotating the pipe section upstream the bend. The mean field was presented for swirl numbers from $S = 0$ to 1.2 from the PIV data, showing that the secondary motion in a curved pipe gradually diminishes as the swirl number increases. The flow field becomes more symmetric with increasing swirl intensity and approaches that in a straight pipe flow with the two Dean cells merging into a single cell spanning the whole cross-section for $S = 1.2$. The single hot-wire was found to provide a satisfactory estimate of the streamwise velocity for the non-swirling case, however for the highest swirl rate where curvature effects have been damped, the agreement between the HW and TS-PIV data was significantly improved. The swirling motion was found here to have a damping effect on the turbulence, as it is known for straight pipe flow, even after the bend. The present work is believed to make unique data available for—but

not only—validation of CFD codes. The data, from both the hot-wire and PIV measurements, can be obtained from the authors.

References

Al-Rafai WN, Tridimas YD, Woolley NH (1990) A study of turbulent flows in pipe bends. Proc Inst Mech Eng Part C 204:399–408

Anwer M, So RMC (1993) Swirling turbulent flow through a curved pipe. Part 1: effect of swirl and bend curvature. Exp Fluids 14:85–96

Anwer M, So RMC, Lai YG (1989) Perturbation by and recovery from bend curvature of a fully developed turbulent pipe flow. Phys Fluids 1:1387

Azzola J, Humprey JAC, Iacovides H, Launder BE (1986) Developing turbulent flow in a U-bend of circular cross-section: measurement and computation. J Fluids Eng 108:214–221

Binnie AM (1962) Experiments on the swirling flow of water in a vertical pipe and a bend. Proc R Soc 270:452–466

Boersma BJ, Nieuwstadt FTM (1996) Large-eddy simulation of turbulent flow in a curved pipe. J Fluids Eng 118:248–254

Brücker C (1998) A time-recording DPIV-Study of the swirl switching effect in a 90° bend flow. In: Proceedings of 8th international symposium on flow visualization, 1–4 Sept 1998, Sorrento, NA, Italy

Bruun H (1995) Hot-wire anemometry: principles and signal analysis. Oxford University Press, Oxford

Carlsson C (2014) Utilization of decomposition techniques for analyzing and characterizing flows. PhD Thesis, Lund University, Lund, Sweden

Chandran KB, Yearwood TL (1981) Experimental study of physiological pulsatile flow in a curved tube. J Fluid Mech 111:59–85

Chang TH (2003) An investigation of heat transfer characteristics of swirling flow in a 180° circular section bend with uniform heat flux. J Mech Sci Technol 17:1520–1532

Chang TH, Lee HS (2003) An experimental study on swirling flow in a 90 degree circular tube by using particle image velocimetry. J Vis 6:343–352

Dean WR (1927) Note on the motion of fluid in a curved pipe. Phil Mag 4:208–223

Eggels J (1994) Direct and large eddy simulation of turbulent flow in a cylindrical geometry. PhD Thesis, Delft Univeristy of Technology, Delft, The Netherlands

Enayet MM, Gibson MM, Taylor A, Yianneskis M (1982) Laser-Doppler measurements of laminar and turbulent flow in a pipe bend. Int J Heat Fluid Flow 3:213–219

Facciolo L (2006) A study on axially rotating pipe and swirling jet flows. PhD Thesis, KTH Mechanics, Stockholm, Sweden

Facciolo L, Tillmark N, Talamelli A, Alfredsson PH (2007) A study of swirling turbulent pipe and jet flows. Phys Fluids 19:035105

Feiz AA, Ould-Rouis M, Lauriat G (2003) Large eddy simulation of turbulent flow in a rotating pipe. Int J Heat Fluid Flow 24:412–420

Fjällman J, Mihaescu M, Fuchs L (2013) Analysis of secondary flow induced by a 90° bend in a pipe using mode decomposition techniques. 4th international conference on jets, wakes and separated flows, 17–21 Sept 2013, Nagoya, Japan

Glenn AL, Bulusu K, Shu F, Plesniak MW (2012) Secondary flow structures under stent-induced perturbations for cardiovascular flow in a curved artery model. Int J Heat Fluid Flow 35:76–83

Gupta AK, Lilley DG, Syred N (1985) Swirl flows. ABACUS Press, Cambridge

Hellström F (2010) Numerical computations of the unsteady flow in turbochargers. PhD Thesis, KTH Mechanics, Stockholm, Sweden

Hellström LHO, Zlatinov M, Cao G, Smits A (2013) Turbulent pipe flow downstream of a 90° bend. J Fluid Mech 735:R7

Helps EPW, McDonald DA (1954) Observations on laminar flow in veins. J Physiol 124:631–639

Hüttl TJ, Friedrich R (2001) Direct numerical simulation of turbulent flows in curved and helically coiled pipes. Comput Fluids 30:591–605

Imao S, Itoh M, Harada T (1996) Turbulent characteristics of the flow in an axially rotating pipe. Int J Heat Fluid Flow 17:444–451

Ito H, Nanbu K (1971) Flow in rotating straight pipes of circular cross section. J Basic Eng 93:383–394

Jakirlić S, Hanjalić K, Tropea C (2002) Modeling rotating and swirling turbulent flows: a perpetual challenge. AIAA J 40:1984–1996

Kadyirov A (2013) Numerical investigation of swirl flow in curved tube with various curvature ratio. In: Proceedings of COMSOL Conference 23–25 Oct 2013, Rotterdam, The Netherlands

Kalpakli A, Örlü R (2013) Turbulent pipe flow downstream a 90° pipe bend with and without superimposed swirl. Int J Heat Fluid Flow 41:103–111

Kalpakli A, Örlü R, Alfredsson PH (2013) Vortical patterns in turbulent flow downstream a 90° curved pipe at high Womersley numbers. Int J Heat Fluid Flow 44:692–699

Kalpakli A, Örlü R, Alfredsson PH (2012) Dean vortices in turbulent flows: rocking or rolling? J Vis 15:37–38

Kalpakli Vester A, Örlü R, Alfredsson PH (2015) POD analysis of the turbulent flow downstream a mild and sharp bend. Exp Fluids 56:57

Kalpakli A, Örlü R, Tillmark N, Alfredsson PH (2012) Experimental investigation on the effect of pulsations on exhaust manifold-related flows aiming at improved efficiency. In: Proceedings of 10th international conference on turbochargers and turbocharing, 15–16 May, London, UK, pp 377–387

Kikuyama K, Murakami M, Nishibori K (1983a) Development of three-dimensional turbulent boundary layer in an axially rotating pipe. Trans Inst Chem Eng 105:154–160

Kikuyama K, Murakami M, Nishibori K, Maeda K (1983b) Flow in an axially rotating pipe: a calculation of flow in the saturated region. Bull JSME 26:506–513

Kitoh O (1987) Swirling flow through a bend. J Fluid Mech 175:429–446

Murakami M, Kikuyama K (1980) Turbulent flow in axially rotating pipes. J Fluids Eng 102:97–103

Noorani A, Schlatter P (2015) Evidence of sublaminar drag naturally occurring in a curved pipe. Phys Fluids 27:035105

Noorani A, El Khoury GK, Schlatter P (2013) Evolution of turbulence characteristics from straight to curved pipes. Int J Heat Fluid Flow 41:16–26

Nygård F, Andersson HI (2009) DNS of swirling turbulent pipe flow. Int J Num Methods Fluids 64:945–972

Ono A, Kimura N, Kamide H, Tobita A (2010) Influence of elbow curvature on flow structure at elbow outlet under high Reynolds number condition. Nucl Eng Design 241:4409–4419

Orlandi P, Fatica M (1997) Direct simulations of turbulent flow in a pipe rotating about its axis. J Fluid Mech 343:43–72

Örlü R (2009) Experimental studies in jet flows and zero pressure-gradient turbulent boundary layers. PhD Thesis, KTH Mechanics, Stockholm, Sweden

Örlü R, Alfredsson PH (2007) An experimental study of the near-field mixing characteristics of a swirling jet. Flow Turb Combust 80:323–350

Örlü R, Alfredsson PH (2012) Comment on the scaling of the near-wall streamwise variance peak in turbulent pipe flows. Exp Fluids 54:1431

Pruvost J, Legrand J, Legentilhomme P (2004) Numerical investigation of bend and torus flows, part I: effect of swirl motion on flow structure in U-bend. Chem Eng Sci 59:3345–3357

Reich G, Beer H (1989) Fluid flow and heat transfer in an axially rotating pipe—I. Effect of rotation on turbulent pipe flow. Int J Heat Mass Transfer 32:551–562

Rocklage-Marliani G, Schmidts M, Vasanta Ram V (2003) Three-dimensional laser-Doppler velocimeter measurements in swirling turbulent pipe flow. Flow Turb Combust 70:43–67

Röhrig R, Jakirlić S, Tropea C (2015) Comparative computational study of turbulent flow in a 90° pipe elbow. Int J Heat Fluid Flow. doi:10.1016/j.ijheatfluidflow.2015.07.011

Rütten F, Schröder W, Meinke M (2005) Large-eddy simulation of low frequency oscillations of the Dean vortices in turbulent pipe bend flows. Phys Fluids 17:035107

Sakakibara J, Machida N (2012) Measurement of turbulent flow upstream and downstream of a circular pipe bend. Phys Fluids 24:041702

Shirvan SS (2011) Experimental study of complex pipe flows. Master Thesis, KTH Mechanics, Stockholm, Sweden

Shimizu Y, Sugino K (1980) Hydraulic losses and flow patterns of a swirling flow in U-bends. JSME 23:1443–1450

So R, Anwer M (1993a) Fully-developed turbulent flow through a curved pipe with and without swirl. ASME-FED 146:29–29

So RMC, Anwer M (1993b) Swirling turbulent flow through a curved pipe. Part 2: recovery from swirl and bend curvature. Exp Fluids 14:169–177

Speziale CG, Younis BA, Berger SA (2000) Analysis and modelling of turbulent flow in an axially rotating pipe. J Fluid Mech 407:1–26

Sudo K, Sumida M, Hibara H (1998) Experimental investigation on turbulent flow in a circular-sectioned 90° bend. Exp Fluids 25:42–49

Tunstall MJ, Harvey JK (1968) On the effect of a sharp bend in a fully developed turbulent pipe-flow. J Fluid Mech 34:595–608

Vashisth S, Kumar V, Nigam KDP (2008) A review on the potential applications of curved geometries in process industry. Ind Eng Chem Res 47:3291–3337

Westerweel J (1994) Efficient detection of spurious vectors in particle image velocimetry data. Exp Fluids 16:236–247

White A (1964) Flow of a fluid in an axially rotating pipe. J Mech Eng Sci 6:47–52

Wieneke B (2005) Stereo-PIV using self-calibration on particle images. Exp Fluids 39:267–280

Wu X, Moin P (2008) A direct numerical simulation study on the mean velocity characteristics in turbulent pipe flow. J Fluid Mech 608:81–112

Yamano H, Tanaka M, Murakami T, Iwamoto Y, Yuki K, Sago H, Hayakawa S (2011) Unsteady elbow pipe flow to develop a flow-induced vibration evaluation methodology for Japan sodium-cooled fast reactor. J Nucl Sci Technol 48:677–687

Yuki K, Hasegawa S, Sato T, Hashizume H, Aizawa K, Yamano H (2011) Matched refractive-index PIV visualization of complex flow structure in a three-dimensionally connected dual elbow. Nucl Eng Design 241:4544–4550